Matthew Pihowich

Microfluidics Lab

Introduction

Flow Dynamics in a microfluidic environment is a vastly important area of study in numerous fields. In biology for example, microfluidics is used for stem cell research, drug development, and as modeling for various important biological functions [1]. This paper aims to utilize microfluidic flow to validate several accepted theoretical models in Fluid Dynamics including velocity gradients, Bernoulli's equation, conservation of mass, and the qualitative behavior of fluid flow. Bernoulli's equation can firstly be given below in Equation 1, where the flow is assumed to be frictionless, steady, incompressible, and states that this formula of pressure p, density ρ, velocity V, gravitational constant g, and relative height h is constant along a streamline. The formula for the conservation of mass is given by Equation 2 where A is the cross-sectional area of the curve and V and ρ are like before. In addition, it is expected that the velocity profile of a fluid flowing against a boundary is shows a parabolic shape near the boundary with a no-slip condition at the boundary where the velocity equals zero [2]

$$p + \frac{1}{2}\rho V^2 + \rho g h = Const \quad (1)[3]$$

$$\rho A_1 V_1 = \rho A_2 V_2 \quad (2)[4]$$

Experimental Procedures

The procedure as stated in the lab manual [5] was followed to collect data in the form of microscopic images with variable exposure lengths. The photos were then analyzed using Microsoft Paint to determine the speed of each particle by measuring the length of the particle's path in pixels. The distance between the x-coordinates and the distance between the y-coordinates of the particle trails were measured. The magnitude of these values was then taken as seen in Equation 3.

$$D_{tot}\,[px] = \sqrt{(D_x)^2 + (D_y)^2} \quad (3)$$

Then the scale factor of the image was calculated as seen in Equation 4, where the reported length of the scale in μm was divided by the length of the line, similarly as measured as with the particle trails.

$$S\left[\frac{\mu m}{px}\right] = \frac{L_{scale}}{D_{tot}} = \frac{301.6\ \mu\text{m}}{467\ px} = 0.6458\ \frac{\mu\text{m}}{px} (4)$$

The reported measurements of the distance in pixels were converted by multiplying by the scaling factor. These values were then divided by the exposure to give the speed of the particles as seen in Equation 5.

$$V = \frac{D_{tot}}{t_{exp}} \quad (5)$$

Error Analysis

For length, each measurement in Microsoft Paint has a y and x-direction uncertainty of ±1 pixel. Thus, using Formula 6 below, the uncertainty in any measured distance in one dimension is ±1.7 pixels [6].

$$\Delta D_x = \sqrt{(\Delta x_1)^2 + (\Delta x_2)^2} = \sqrt{(1)^2 + (1)^2} \sim 1.7\ px \quad (6)$$

Furthermore, taking the magnitude of the x and y direction values for total distance as seen in Equation 3, the uncertainty in the total measurement can be seen using the partials of this equation and inputting them into the partial definition of uncertainty as seen in Equation 5 [6].

$$\Delta D_{tot} = \sqrt{\left(\frac{D_x \Delta D_x}{\sqrt{(D_x)^2 + (D_y)^2}}\right)^2 + \left(\frac{D_y \Delta D_y}{\sqrt{(D_x)^2 + (D_y)^2}}\right)^2} \quad (5)$$

Then to find the uncertainty of the length scale S from Equation 4 where L_{scale} is the length of the scale in µm, the uncertainty relation and a sample calculation can be seen in Equation 8 [6].

$$\Delta S = S\sqrt{\left(\frac{\Delta L_{scale}}{L_{scale}}\right)^2 + \left(\frac{\Delta D_{tot}}{D_{tot}}\right)^2} = \sqrt{\left(\frac{0.05}{301.6}\right)^2 + \left(\frac{467}{1.7}\right)^2} = 0.0020\ \frac{\mu m}{px} \quad (8)$$

Thus, the total uncertainty in the distance in µm can be found using Equation 9 [6].

$$\Delta D_{tot}[\mu m] = D_{tot}\sqrt{\left(\frac{\Delta S}{S}\right)^2 + \left(\frac{\Delta D_{tot}[px]}{D_{tot}[px]}\right)^2} = \quad (9)$$

The uncertainty in time is given by the measurement of the exposure time, half of the digit after the recorded time. For all exposure times, the uncertainty was ±0.05ms. Thus, the uncertainty in the velocity can be found in Equation 10 using time t and D_{tot} in µm.

$$\Delta V = V\sqrt{\left(\frac{\Delta D_{tot}}{D_{tot}}\right)^2 + \left(\frac{\Delta t}{t}\right)^2} \quad (10)$$

In addition, there are several variables that should be noted in the possibility of causing uncertainty in these measurements. Notably, there were large obstacles at certain locations in the tubes, an example of which can be seen in Figure 1. In addition, the edges of the tubes appear to be unsmooth, with several imperfections, as well as a noticeable velocity gradient near the edges.

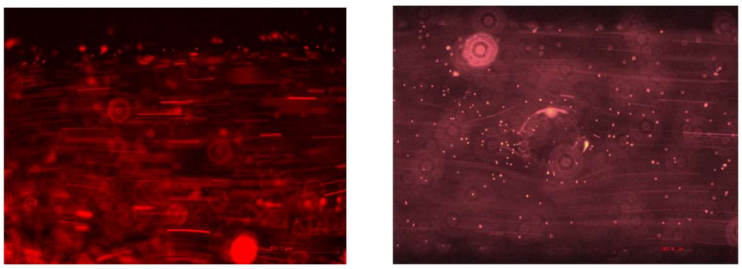

Figure 1: Image at edge of straight wall on the left and image of disturbance on the right.

Results and Discussion

The velocity in the straight channel would be expected to be the largest in the center of the channel. This is where the flow is the least impeded by the edge of the channel, and the flow velocity will gradually decrease as it gets closer to the wall to a theoretical value of zero. This would be the largest difference in the velocity is present. The actual measured curve is given below in Figure 2.

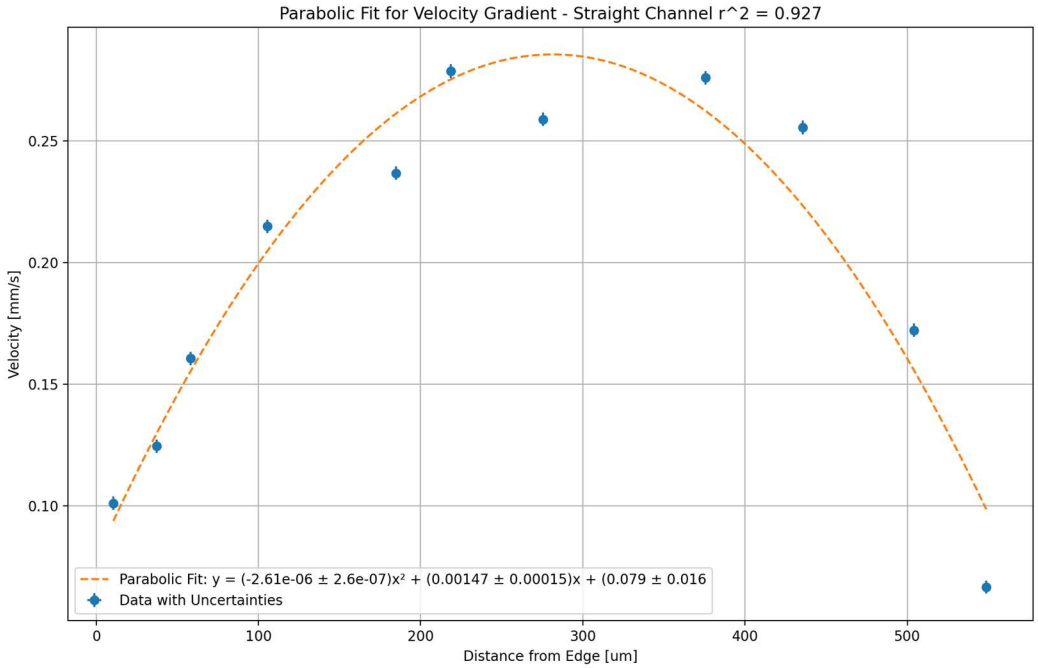

Figure 2: Parabolic fit for velocity gradient with an r^2 value of 0.927.

The ability for the velocity gradient to be reasonably represented by a parabolic function agrees with the expectation above and supports the theoretical relationship.

This velocity can be further manipulated by changing the height at which the syringe is above the chip or by adding pressure seen in Equation 11, derived from Equation 1. By setting up the equation for two related points as seen below and solving for the change in velocity, it is possible to see the relationship between a change in height and a change in velocity should follow a square root function. In this case, pressure is also a linear function of height, so the change in velocity should be able to be modeled by a square root function as given by Equation 12 where velocity is in meters per second and h is in meters. This comes with Bernoulli's equation assumptions, notably that the flow is frictionless, steady, and incompressible, which are not completely satisfied in real life.

$$p_1 + \frac{1}{2}\rho {V_1}^2 + \rho g h_1 = p_2 + \frac{1}{2}\rho {V_2}^2 + \rho g h_2 \quad (11)$$

$$\Delta V = \sqrt{\frac{2}{\rho}(\rho g \Delta h + \Delta p)} = \sqrt{\frac{2}{\rho}(\rho g \Delta h + \rho g \Delta h)} = 2\sqrt{g \Delta h} = 6.26\sqrt{\Delta h} \quad (12)$$

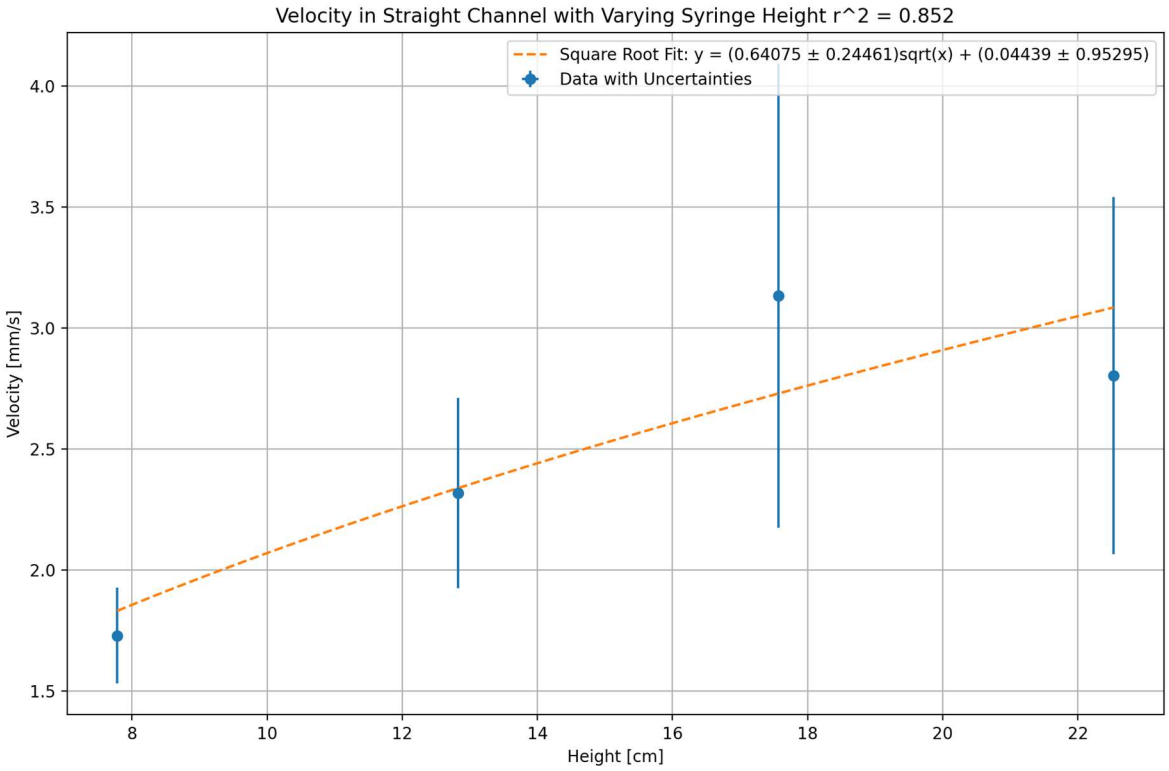

Figure 3: Square root fit for velocity with a dependence on height with an r^2 value of 0.852.

The experimental result as shown in Figure 3 shows support for this theory. A square root function is shown to represent the trend quite well with a correlation of 0.852. In addition, the y-intercept is within uncertainties of zero, which is concurrent with the theoretical relationship. Adjusting for units, the value of the constant to the square root factor is 6.4±2.4. this has a high level of uncertainty due to the varying levels of velocity in the straight channel, but this average value lies within uncertainties of the theoretical model.

Channels of Different Size

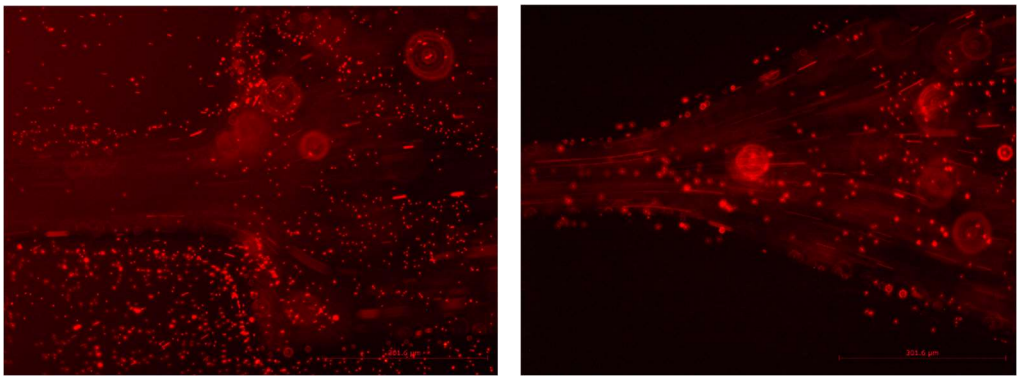

Figure 4: Abrupt change in channel width and gradual change in channel width.

Abrupt Change		
Largest Area Velocity	Thin Tube Velocity	Expected Thin Tube Velocity
0.27377 ± 0.00059 mm/s	0.7557 ± 0.0016 mm/s	1.176 ± 0.0044 mm/s

Table 1: Thin tube velocity, largest area velocity, and expected thin tube velocity in the channel with abrupt change.

Gradual Change		
Largest Area Velocity	Thin Tube Velocity	Expected Thin Tube Velocity
1.072 ± 0.0025 mm/s	4.10 ± 0.01 mm/s	4.77 ± 0.02 mm/s

Table 2: Thin tube velocity, largest area velocity, and expected thin tube velocity in the channel with gradual change.

Expected thin tube Velocity was calculated using the velocity in the largest area and applying the principles of conservation of mass as seen earlier in Equation 2. The assumption in this case is that equal mass is flowing in and out of the region, with the fluid being incompressible, frictionless, and steady. The result of this calculation can be seen in the above tables. Notably, both expected values are near but greater than the actual recorded values of velocity in the channels. This is most likely due to the not completely valid assumptions that were present in the calculation.

The most pronounced difference between these two flows is the presence of turbulent flow in the abrupt channel. While the gradual channel maintained relative steady and laminar flow, the abrupt channel, as seen in Figure 4, had notable areas that were stagnant or turbulent in the corners near the abrupt change. This exhibits one reason why flow transitions are so common in the working world: greater energy efficiency. The flow in the gradual channel does not lose as much energy to the turbulence and as such carries more energy with it. Steady flow is also more predictable than turbulent flow, which is another reason it could be preferred for engineers.

Channels with Bends

The flow velocity should theoretically be the same before and after the bends in the tubes because the density and flow area should be the same with reference to the conservation of mass as seen in Equation 2. However, this was not measured, possibly due to random chance in the recorded particles or with problems in the assumptions made, specifically incompressible flow and this possibility for viscous forces. The experimental data show that the flow did indeed slow down during the bend but struggled to reapproach the same velocity.

Sine Bend		
Before Velocity	Peak Velocity	After Velocity
1.594 ± 0.014 mm/s	1.003 ± 0.014 mm/s	1.039 ± 0.014 mm/s

Table 3: Velocity taken before, during, and after Sine Bend.

Square Bend		
Before Velocity	Peak Velocity	After Velocity
1.307 ± 0.014 mm/s	0.734 ± 0.014 mm/s	1.021 ± 0.02 mm/s

Table 4: Velocity taken before, during and after Square Bend.

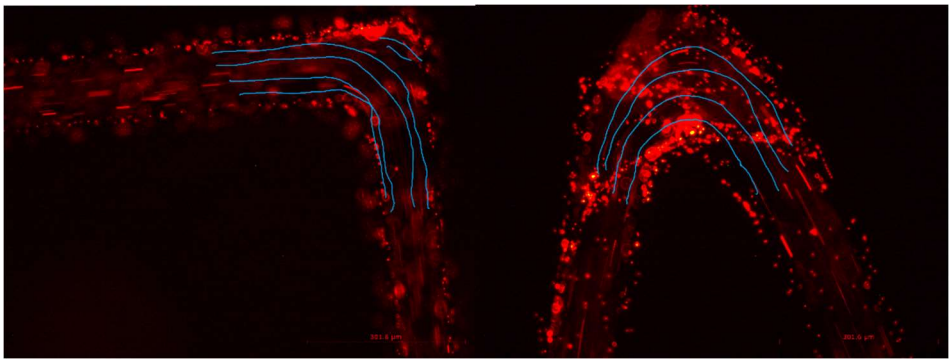

Figure 5: Flow around a sine curve and an abrupt curve with path lines drawn.

The flow is relatively steady and laminar in the tubes as seen in Figure 5. The velocity in both before and after is the same due to the conservation of mass as previously stated. The only difference between the sharp and smooth bends occurs at the turns in the channels. The smooth bend generally retains its steadiness, but the square bend has a notable section of turbulence at the very corner. There are not many particles traveling in and out of this section. Path lines for these flows can be seen in Figure 5.

Conclusions

This paper has aimed to confirm the application of several notable theoretical models in the space of Fluid Dynamics, notably Bernoulli's equation, the behavior of fluid in velocity profiles, as well as the conservation of momentum in fluids. Bernoulli's equation was shown to be accurate with a relationship between height and velocity where the experimental constant 6.4±2.4 was within uncertainties of the real value of 6.26. In addition, the behavior of the velocity profile was confirmed to be parabolic in nature with a correlation of 0.927 for the parabolic model. Finally, the conservation of momentum was determined to be relatively correct from the experiment with changing cross-sections and changing curve shapes, albeit with some significant deviations most likely due to assumptions such as incompressibility, no friction, and steady flow that may not hold in these situations. However, even with these slight deviations, all theories chosen to verify in this paper have been shown to provide a decent approximation of the real world.

References

[1] S. Cheriyedath, "Microfluidics applications," News, https://www.news-medical.net/life-sciences/Microfluidics-Applications.aspx (accessed Nov. 29, 2023).
[2] "Flows with friction," Princeton University, https://www.princeton.edu/~asmits/Bicycle_web/frictionflows.html (accessed Nov. 29, 2023).
[3] "Bernoulli's equation," Princeton University, https://www.princeton.edu/~asmits/Bicycle_web/Bernoulli.html (accessed Nov. 29, 2023).
[4] "Conservation of mass," NASA, https://www.grc.nasa.gov/www/k-12/airplane/mass.html (accessed Nov. 29, 2023).
[5] B. Keith, E. Chung, T. Dell, P. Deng, and Z. Lu, *Microfluidics Lab Manual*. Toronto, ON: University of Toronto, 2023.
[6] PHY293, *Uncertainty Propagation Formulae*. Toronto, ON: University of Toronto, 2023.